

Nonlinear Valley Hall Effect


Kamal Das^{1,2,*}, Koushik Ghorai,¹ Dimitrie Culcer,^{3,4} and Amit Agarwal^{1,†}

¹Department of Physics, Indian Institute of Technology, Kanpur-208016, India

²Department of Condensed Matter Physics, Weizmann Institute of Science, Rehovot 7610001, Israel

³School of Physics, The University of New South Wales, Sydney 2052, Australia

⁴ARC Centre of Excellence in Future Low-Energy Electronics Technologies,
The University of New South Wales, Sydney 2052, Australia

 (Received 3 August 2023; revised 16 December 2023; accepted 26 January 2024; published 28 February 2024)

The valley Hall effect arises from valley-contrasting Berry curvature and requires inversion symmetry breaking. Here, we propose a nonlinear mechanism to generate a valley Hall current in systems with both inversion and time-reversal symmetry, where the linear and second-order charge Hall currents vanish along with the linear valley Hall current. We show that a second-order valley Hall signal emerges from the electric field correction to the Berry curvature, provided a valley-contrasting anisotropic dispersion is engineered. We demonstrate the nonlinear valley Hall effect in tilted massless Dirac fermions in strained graphene and organic semiconductors. Our Letter opens up the possibility of controlling the valley degree of freedom in inversion symmetric systems via nonlinear valleytronics.

DOI: [10.1103/PhysRevLett.132.096302](https://doi.org/10.1103/PhysRevLett.132.096302)

Introduction.—Comprehending and controlling diverse degrees of freedom in quantum materials not only enriches our understanding of fundamental physics, it also paves the way for novel applications. For example, the fields of electronics and spintronics emerged from understanding and exploiting the charge and spin degree of freedom [1,2], respectively. Beyond these, the valley degree of freedom has attracted significant attention giving birth to the field of valleytronics [3–5]. Valleys are the degenerate energy extrema of the electronic bands in momentum space. Valleys become well-defined degrees of freedom when they are well separated in momentum space with negligible intervalley scattering. The primary focus of valleytronics is to control and manipulate the valley degree of freedom by using electrical [6–9], optical [10–13], and magnetic [14–16] means.

The linear valley Hall effect (VHE) introduced by Xiao *et al.* [6] enables electrical control and manipulation of the valley degree of freedom. VHE is the accumulation of electrons with opposite valley indices on opposite sides of a sample, transverse to the direction of the applied electric field. It is induced by the valley-contrasting Berry curvature and anomalous Hall velocity in materials with broken inversion symmetry. It offers a way to probe the Berry curvature in time-reversal-preserving systems where the anomalous charge Hall response vanishes. VHE has been measured via nonlocal resistance measurements in hexagonal graphene superlattices [7–9] and in monolayer transition metal dichalcogenides [17]. However, in systems with inversion and time-reversal symmetry, the Berry curvature vanishes for each point in momentum space, leading to the absence of VHE in such systems. This raises

a fundamental question. How can we probe and manipulate the valley degree of freedom in nonmagnetic and inversion symmetric materials by electrical means?

Here, we demonstrate that the nonlinear valley Hall effect (NVHE) can probe and manipulate the valley degree of freedom in inversion and time-reversal symmetric systems. We show that materials with both fundamental symmetries exhibit a finite NVHE that is second order in the electric field (see Fig. 1), provided their band dispersion

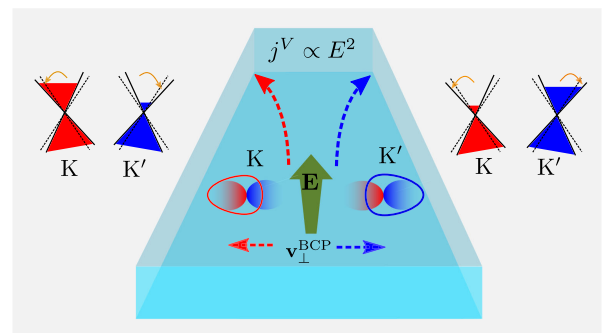


FIG. 1. Schematic of the nonlinear valley Hall effect. A longitudinal electric field induces a nonlinear valley Hall current ($j^V \propto E^2$). Because of the Berry-connection-polarizability (BCP) induced Hall velocity, electrons near the Fermi surface with different valley degrees of freedom accumulate on opposite sides of the sample. The elliptical density shows the BCP-induced Hall velocity distribution, and the contours show the Fermi surfaces. The nonlinear valley Hall effect is finite in inversion and time-reversal symmetric systems such as tilted gapless graphene, where the linear valley response and linear and nonlinear charge responses vanish.

is anisotropic and valley contrasting [18–20]. Such a dispersion can be engineered by reducing crystalline symmetries while retaining inversion and time-reversal symmetry, via strain or other means. The NVHE originates from the electric-field-induced correction to the Berry curvature, which results in a nonlinear anomalous Hall velocity. Since the electric field correction is determined by the Berry connection polarizability (BCP) [21,22], the NVHE can be used to investigate the quantum metric in systems with both fundamental symmetries.

We demonstrate that the charge carriers of opposite valleys carry opposite signs of the electric-field-induced orbital magnetic moment (OMM). Thus, the NVHE separates carriers with opposite electric-field-induced OMM, even though the total field-induced orbital magnetization vanishes in the system. Additionally, we highlight the intrinsic (scattering-time-independent) nature of the NVHE and show that the dominant part of the disorder-induced extrinsic contributions in NVHE vanish for the tilted Dirac Hamiltonian. Experimentally, the NVHE can be probed via nonlocal resistance measurements using the scaling of the nonlocal resistance with the longitudinal Ohmic resistivity, which is different from the linear VHE. As specific examples, we demonstrate the existence of NVHE in strained graphene, which hosts tilted massless Dirac fermions, and in the organic semiconductor α (BEDT-TTF) $_2$ I $_3$ [BEDT-TTF = bis(ethylenedithio) tetrathiafulvalene].

Theory of nonlinear valley Hall effect.—The linear valley Hall current (j_a^V) is defined in terms of the linear valley Hall conductivity (σ_{ab}^V) as $j_a^V = \sigma_{ab}^V E_b$. Here, $j_a^V = j_a^K - j_a^{K'}$ and $\sigma_{ab}^V = \sigma_{ab}^K - \sigma_{ab}^{K'}$, with the distinct valleys specified by K and K'. Under time reversal, the valley current ($j_a^K \rightarrow -j_a^{K'}$ and $j_a^{K'} \rightarrow -j_a^K$) and the electric field do not change sign. However, under space inversion, the valley current remains unchanged, but the electric field changes sign. These symmetry considerations force the linear valley Hall current to vanish in an inversion symmetric system. In this background, we introduce the notion of NVHE originating from the nonlinear charge response specified by $j_a^{(2)} = \chi_{a;bc} E_b E_c$. We define the valley-resolved nonlinear charge conductivity as $j_a^{V(2)} = \chi_{a;bc}^{\text{NLV}} E_b E_c$, where

$$\chi_{a;bc}^{\text{NLV}} = \chi_{a;bc}^K - \chi_{a;bc}^{K'}. \quad (1)$$

In an inversion symmetric system, the second-order nonlinear charge current vanishes, and the dominant valley response is the nonlinear valley Hall current [23].

The origin of the NVHE can be understood from the semiclassical electron dynamics by incorporating corrections up to second order in the electric field [21,24]. In the nonlinear regime, the anomalous Hall velocity $v_{\text{AHE}} = (e/\hbar)\mathbf{E} \times \boldsymbol{\Omega}_n$ arising from the interband coherence gets a nonlinear correction induced by the external electric field.

The modification yields $v_{\text{AHE}} \rightarrow v_{\text{AHE}}^E = (e/\hbar)\mathbf{E} \times (\boldsymbol{\Omega}_n + \boldsymbol{\Omega}_n^E)$ where $\boldsymbol{\Omega}_n = \nabla_{\mathbf{k}} \times \mathcal{A}_n$ is the usual Berry curvature, and $\boldsymbol{\Omega}_n^E$ is an electric-field-induced correction given by

$$\boldsymbol{\Omega}_n^E = \nabla_{\mathbf{k}} \times \mathcal{A}_n^E, \quad \mathcal{A}_{n,a}^E = 2e \sum_{m \neq n} \frac{\text{Re}[\mathcal{R}_{nm}^a \mathcal{R}_{mn}^b]}{\epsilon_n - \epsilon_m} E^b. \quad (2)$$

Here, \mathcal{A}_n^E is an electric-field-induced correction to the Berry connection. The quantity \mathcal{R}_{nm}^a represents the band-resolved Berry connection, and ϵ_n is the eigenvalue of the unperturbed Hamiltonian. To facilitate interpretation, the correction to the Berry connection is expressed as $\mathcal{A}_{n,a}^E = \tilde{\mathcal{G}}_n^{ab} E_b$, where the BCP, $\tilde{\mathcal{G}}_n^{ab}$, is defined as [25]

$$\tilde{\mathcal{G}}_n^{ab} = 2e \sum_{m \neq n} \frac{\text{Re}[\mathcal{R}_{nm}^a \mathcal{R}_{mn}^b]}{\epsilon_n - \epsilon_m}. \quad (3)$$

We emphasize that the BCP contains the band-resolved quantum metric [26,27] $\mathcal{G}_{mn}^{ab} = \text{Re}[\mathcal{R}_{nm}^a \mathcal{R}_{mn}^b]$, which quantifies the distance between wave functions in the parameter space.

In the second order in the electric field, two Hall responses originate from the Berry curvature and the electric-field-induced correction to it. The anomalous Hall velocity combined with the linear nonequilibrium distribution function gives rise to the Berry-curvature-dipole- (BCD) induced nonlinear Hall conductivity [28,29]. It is given by $\chi_{a;bc}^{\text{BCD}} = g_s (e^3 \tau / \hbar^2) \epsilon_{abd} \sum_{n,k} (\partial_c \Omega_n^d) f_n$. Here, f_n is the equilibrium Fermi-Dirac distribution function, τ is quasi-particle scattering time, ϵ_{abd} is the antisymmetric tensor of rank three, and $g_s = 2$ accounts for the spin degeneracy factor. See Sec. S1 of the Supplemental Material [30] for a detailed derivation. The electric field correction to the Berry curvature gives rise to an intrinsic nonlinear Hall current specified by $j_a = -(e^2/\hbar) \epsilon_{abi} \sum_{n,k} E_b (\nabla_k \times \mathcal{A}_n^E)_i f_n$. The corresponding intrinsic nonlinear conductivity is given by [36–41]

$$\chi_{a;bc}^{\text{BCP}} = -g_s \frac{e^2}{2\hbar} \sum_{n,k} \left(2\partial_a \tilde{\mathcal{G}}_n^{bc} - \partial_b \tilde{\mathcal{G}}_n^{ac} - \partial_c \tilde{\mathcal{G}}_n^{ab} \right) f_n. \quad (4)$$

In the presence of inversion symmetry, both of these contributions to the Hall charge current vanish. Below, we show that although the charge current vanishes in systems with both time-reversal and inversion symmetries, the valley-resolved intrinsic contribution survives and generates a finite NVHE.

To understand this, we note that in a spinless system the Berry curvature satisfies $\boldsymbol{\Omega}_n(-\mathbf{k}) = -\boldsymbol{\Omega}_n(\mathbf{k})$ in the presence of time-reversal symmetry, and $\boldsymbol{\Omega}_n(-\mathbf{k}) = \boldsymbol{\Omega}_n(\mathbf{k})$ in the presence of inversion symmetry. As a consequence, when both symmetries are present, $\boldsymbol{\Omega}_n(\mathbf{k}) = 0$ at each point in the momentum space. This forces the linear VHE to vanish. The contribution from the Berry curvature dipole also vanishes for each valley. However, the intrinsic

contribution originating from Eq. (4) for each valley does not vanish and can be finite. The BCP transforms as $\tilde{\mathcal{G}}_n^{ab}(-\mathbf{k}) = \tilde{\mathcal{G}}_n^{ab}(\mathbf{k})$ under the action of both the space inversion and time reversal. Therefore, unlike the Berry curvature, it can be finite at each point in momentum space in the simultaneous presence of both of these symmetries. As a consequence, we can have a nontrivial NVHE. This opens up the potential for controlling the valley degree of freedom in systems with both fundamental symmetries. This is the main highlight of this Letter. The subtle point is that even though both symmetries are preserved globally, they must be broken in the individual valleys (or locally) to obtain a finite NVHE.

Electric-field-induced orbital magnetic moment.— Similar to the spin Hall effect that separates opposite spins, the linear VHE segregates carriers with valley-contrasting OMM in real space by pushing the oppositely OMM polarized carriers to different transverse edges. However, in the presence of both fundamental symmetries, the OMM vanishes in the whole Brillouin zone. This raises a question. What physical quantity distinguishes the carriers separated by the NVHE in real space?

We find that the electric field can induce a correction to the OMM. The a th component of the field-induced OMM for n th band carriers is given by [42,43]

$$m_a^E(n) = \sum_{l \neq n} \left[2e \frac{\text{Re}[\mathcal{M}_{ln}^a \mathcal{R}_{nl}^d]}{\varepsilon_n - \varepsilon_l} + \frac{e^2}{2\hbar} \varepsilon_{abc} (\partial_b \mathcal{G}_{ln}^{cd}) \right] E_d. \quad (5)$$

Here, $\mathcal{M}_{ln} = (e/2) \sum_{j \neq n} (v_{lj} + v_n \delta_{lj}) \times \mathcal{R}_{jn}$ is the inter-band OMM with v_{ij} the matrix element of the velocity operator $\hat{v}^a = (1/\hbar) \partial_a \mathcal{H}$, and we have defined $v_n \equiv v_{nn}$. The NVHE separates carriers with valley-contrasting field-induced OMM given in Eq. (5). We find that materials possessing a valley-contrasting orbital magnetization show the NVHE. See Fig. S1, and Secs. S2 and S3 of the Supplemental Material [30] for a detailed discussion. Below, we show this explicitly for strained graphene and in organic conductors.

Nonlinear valley Hall effect in tilted Dirac systems.— We now demonstrate the NVHE in a two-dimensional tilted Dirac system with two valleys [44]. The system is described by the Hamiltonian,

$$\mathcal{H}(s) = \hbar v_F (s k_x \sigma_x + k_y \sigma_y) + s \hbar v_t k_x \sigma_0. \quad (6)$$

Here, v_F is the Fermi velocity, and σ_i 's are the Pauli matrices representing the sublattice degree of freedom. In Eq. (6), $s = \pm 1$ denotes the valley index, and the \mathbf{k} for each valley is measured from the two Dirac points located at the K or K' point. The v_t term tilts the Dirac cone along the k_x axis in opposite directions for the two valleys. The tilt term breaks the space-inversion and time-reversal symmetries for each valley as $\varepsilon(-\mathbf{k}) \neq \varepsilon(\mathbf{k})$. However, the pair of

oppositely tilted Dirac nodes preserves both the fundamental symmetries globally.

The energy dispersion for this two-band model is given by $\varepsilon_\lambda = s \hbar v_t k_x + \lambda \hbar v_F k$, with $k = (k_x^2 + k_y^2)^{1/2}$, and $\lambda = \pm 1$ denotes the band index. The z component of the Berry curvature for this system vanishes in the entire Brillouin zone. We calculate the elements of the quantum metric to be $\mathcal{G}_{cv}^{xx} = \mathcal{G}_{vc}^{xx}$ and $\mathcal{G}_{cv}^{yy} = \mathcal{G}_{vc}^{yy}$, with

$$\mathcal{G}_{cv}^{xx} = \frac{k_y^2}{4k^4}, \quad \mathcal{G}_{cv}^{yy} = \frac{k_x^2}{4k^4}, \quad \text{and} \quad \mathcal{G}_{cv}^{xy} = \mathcal{G}_{vc}^{xy} = -\frac{k_x k_y}{4k^4}. \quad (7)$$

We note that the quantum metric is independent of the tilt velocity and the valley index. Furthermore, in contrast to the Berry curvature, the sublattice (or inversion) symmetry-breaking gap parameter is not needed to have a finite quantum metric.

We calculate the valley and band-resolved nonlinear Hall conductivity to be $\chi_{x:yy}^{\text{BCP}}(s, \lambda) = -s \lambda (e^3 v_t / 4 \pi \mu^2)$. This is in the limit of small tilt velocity $v_t \ll v_F$ for the chemical potential μ measured from the Dirac point. The valley dependence (captured by $s = \pm 1$) in the valley-resolved nonlinear intrinsic Hall current leads to the accumulation of the electrons with opposite valley index on the opposite side of the samples. This results in NVH conductivity,

$$\chi_{x:yy}^{\text{NLV}} = -\lambda \frac{e^3 v_t}{2 \pi \mu^2}. \quad (8)$$

The NVHE depends on the tilt velocity and vanishes as $v_t \rightarrow 0$. This highlights that for each valley, the rotation symmetry (in the continuum model) or the C_3 symmetry (in the lattice model) has to be broken to have a finite NVHE. In experiments, this is achieved via strain or substrate effects. See Sec. S4 of the Supplemental Material [30] for details. To get an estimation of the strength of the NVHE, we define the NVH angle as $\theta^{\text{NLV}} = j^{\text{V}(2)} / j_L$, where j_L is the linear longitudinal current. For the typical value of model parameters $v_t = 0.3 v_F$ with $v_F = 10^6$ m/s, $\mu = 0.1$ eV, $\tau = 1$ ps, and $E \sim 1$ V/ μm , we find that the NVH angle is $\theta^{\text{NLV}} \approx 0.006\%$. See Sec. S4(C) in the Supplemental Material [30] for details. The NVHE with a different type of band anisotropy and trigonal warping has been demonstrated in Sec. S5 in the Supplemental Material [30].

We can interpret our result of Eq. (8) as an accumulation of carriers with valley-contrasting electric-field-induced OMM along the edge of the sample. For $\mathbf{E} = E_y \hat{y}$, using Eq. (7) in Eq. (5), we calculate

$$m_z^E(s, \lambda) = -\frac{e^2 k_x}{8 \hbar k^4} \left(1 - 2 \lambda s \frac{v_t k_x}{v_F k} \right) E_y. \quad (9)$$

Integrating this equation, we find that the total electric-field-induced OMM for the two valleys is equal in magnitude with

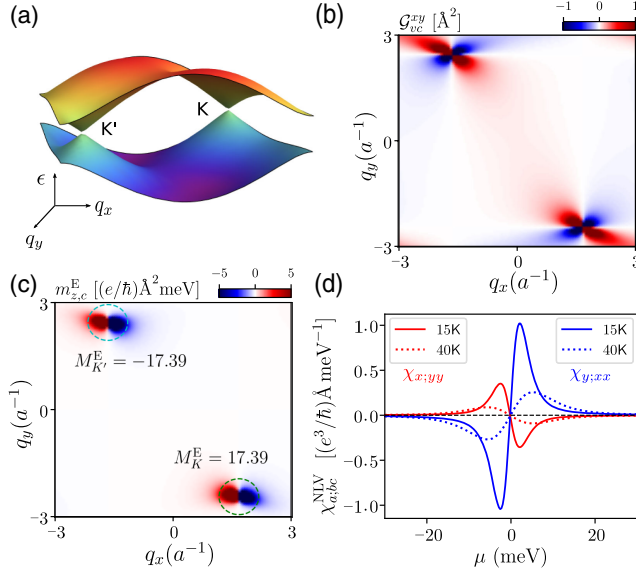


FIG. 2. (a) The electronic dispersion showing the two valleys of organic conductor $\alpha(\text{BEDT-TTF})_2\text{I}_3$. The momentum space distribution of (b) the band-resolved quantum metric, and (c) the electric-field-induced orbital magnetic moment for the conduction band. We have highlighted the valley-contrasting orbital magnetization (M_K^E) of the valleys. (d) Nonlinear valley Hall conductivities induced by the Berry connection polarizability for two representative temperatures: 15 and 40 K. We have offset the energy axis by -92 meV so that $\mu = 0$ represents the band touching point. We have used the following Hamiltonian parameters: $\{t_1, t'_1, t_2, t'_2, t_{\text{nnn}}\} = \{36, -86, -24, -77, -60\}$ meV for our numerical calculations.

opposite signs, $M_a^E(s, n) = \int_{K_s} m_a^E(s, n) f_n \propto s$. Here, \int_{K_s} represents the integration near the valleys. Going beyond the low energy description, we also demonstrate the opposite orbital magnetization of the two valleys for an organic conductor in Fig. 2(c) and in the tight-binding model of strained graphene in Fig. S7(c) of the Supplemental Material [30].

Intrinsic contributions to the valley Hall effect.—For the linear VHE, in addition to the Berry-curvature-induced intrinsic contribution, there are also finite extrinsic contributions induced by asymmetric scattering due to disorder [45]. Such extrinsic contributions arise from the side-jump and skew-scattering mechanisms [46,47]. Intriguingly, these extrinsic contributions are known to sometimes partially compensate, if not cancel, the intrinsic contribution. This motivates us to explore extrinsic disorder-induced contributions to linear VHE, as well as NVHE predicted in this Letter. Although a detailed disorder calculation within the quantum kinetic theory [48] is deferred to a future publication, we find that both the skew-scattering and side-jump semiclassical contributions vanish in the linear and nonlinear regimes for the Hamiltonian in Eq. (6).

The extrinsic side-jump contribution is determined by the positional shift $\delta \mathbf{r}_{l'l}$ caused by the side-jump process,

which subsequently affects the side-jump velocity $v^{sj} = \sum_{l'} \tilde{\omega}_{l'l}^{\text{sy}} \delta \mathbf{r}_{l'l}$. Here, l and l' represent the quantum state involved in scattering, and $\tilde{\omega}_{l'l}^{\text{sy}}$ is the symmetric scattering probability. Interestingly, the side-jump positional shift is determined by the Berry curvature [45,49]. Hence, in systems with both fundamental symmetries, the principle part of the side-jump contribution is expected to vanish along with the Berry curvature. See Sec. S6(B) of the Supplemental Material [30] for details. On the other hand, the contribution from the skew-scattering mechanism contribution is determined by the asymmetric scattering rate, and it is proportional to the cubic and quartic powers of the scattering potential. This asymmetric scattering also vanishes for the Hamiltonian in Eq. (6) [45,50]. Therefore, in contrast to the linear VHE, the NVHE does not have any contribution from the disorder-induced asymmetric scattering mechanisms for the tilted Dirac model Hamiltonian.

Experimental signature.—The linear VHE has been experimentally probed via two types of measurements. The first approach is based on measuring the anomalous charge Hall response in valley-polarized systems [17,51–53]. The NVHE can be probed via a similar strategy of inducing valley polarization by similar or other means.

Another approach for detecting the VHE is via the nonlocal resistance measurement [7–9,54]. In the presence of a long-range charge neutral valley Hall signal, the nonlocal resistance generated by the inverse VHE scales as the cubic power of the longitudinal charge resistivity, $(\rho_{xx}^C)^3$. We show that a similar nonlocal Hall measurement setup can also measure the NVHE. However, the scaling of the nonlocal resistance generated by the NVHE will be different from that generated by other means. We calculate the nonlocal resistance originating from the NVHE to be

$$R_{\text{NL}}^{\text{NVHE}}(x) = \frac{W}{2l_v} (\rho_{xx}^C)^5 (\chi_{x,yy}^V)^2 j^2 e^{-|x|/l_v}. \quad (10)$$

Here, W is the width of the sample, l_v is the intervalley scattering length, j is the bias current density used for measurement, and x is the distance from the nominal current path. The calculation details are presented in Sec. S7 of the Supplemental Material [30]. This has to be contrasted with the case when there is no VHE at all, for which we have $R_{\text{NL}}^{\text{no-VH}} \propto \rho_{xx}^C$, and with the case for linear VHE for which we have $R_{\text{NL}}^{\text{linear-VH}} \propto (\rho_{xx}^C)^3 \sigma_{xy}^V$. In contrast to these cases, the nonlocal resistance induced by NVHE is measurement current dependent, and it is proportional to $(\rho_{xx}^C)^5 j^2$. We predict that the NVHE manifests as a second harmonic signal in the nonlocal measurement setup, even though the system has inversion symmetry [55].

Material realization.—As a realistic material example, we calculate the NVHE for the organic conductor $\alpha(\text{BEDT-TTF})_2\text{I}_3$ [61,62] and graphene (graphene results are shown in Sec. S8 of the Supplemental Material [30]) in the presence of uniaxial strain [63,64]. Under strain,

$\alpha(\text{BEDT-TTF})_2\text{I}_3$ supports a pair of oppositely tilted and gapless Dirac cones. It is described by the tight-binding Hamiltonian of the form $\mathcal{H}(\mathbf{q}) = [(h', h^*), (h, h')]$. The off-diagonal elements are given by

$$h(\mathbf{q}) = 2 \left[t_1 e^{iq^+/2} + t'_1 e^{-iq^+/2} + t_2 e^{iq^-/2} + t'_2 e^{-iq^-/2} \right], \quad (11)$$

where $q^\pm = q_x \pm q_y$. Here, t_i and t'_i ($i = 1, 2$) are the nearest neighbor hopping amplitudes (see Sec. S8 of the Supplemental Material [30] for more details). The diagonal elements are given by $h'(\mathbf{q}) = 2t_{\text{nnn}} \cos q_y$, where t_{nnn} is the next neighbor hopping amplitude. We present the resulting electronic dispersion and the corresponding Dirac valleys in Fig. 2(a). In Fig. 2(b), we show the momentum space distribution of the quantum metric. In Fig. 2(c), we display the electric-field-induced OMM which gives rise to valley orbital magnetization. Figure 2(d) illustrates the resulting NVH conductivity. The NVHE decreases as we increase the temperature showing the energy window in which the BCP tensor is finite around the band touching point.

Symmetry and candidate materials.—Nonmagnetic materials with an inversion center are the most suitable candidates for observing NVHE. Note that while the NVHE and intrinsic BCP Hall current [36,37] share the same physical origin, the fundamental symmetries for these two phenomena are mutually exclusive. In addition to the fundamental symmetries, crystalline symmetries like rotation and reflection near the valleys dictate various components of the NVHE tensor, as summarized in Table S1 of Sec. S9 in the Supplemental Material [30]. In gapless systems, the quantum metric peaks near the band crossings. Therefore, symmetry-protected gapless systems are likely to have large NVHE. Furthermore, recent advancements in device technology have enabled the tunability of the band gap in graphene superlattices through gate voltages [8,9,29], facilitating the creation of systems with gapless Dirac nodes on demand. An additional ingredient for inducing a significant NVHE signal is large anisotropy of the Fermi surface. Therefore, strain engineering to distort the Dirac nodes and introduce anisotropy [65] will help observe NVHE. Two-dimensional systems with anisotropic Fermi surface like borophene, the surface states of three-dimensional crystalline topological insulators [66], surface states of the crystalline topological insulator SnTe [67] are good candidates for the observation of NVHE.

Conclusion.—In summary, we have predicted a new valley Hall effect in materials with spatial inversion symmetry. Our findings facilitate the control of the valley degree of freedom in centrosymmetric materials and offer several exciting possibilities. One interesting direction is the field of valley caloritronics utilizing the possibility of the nonlinear valley Nernst effect [68] and nonlinear valley thermal Hall effect. The NVHE can also be generalized to bosonic systems, with possibilities of predicting and observing the magnon contribution to the nonlinear valley

thermal Hall effect [69]. Additionally, nontrivial physics is likely to emerge in spin-orbit coupled systems where the spin-valley coupling has been shown to impact both the spin and valley Hall effect [70].

K. D. thanks Professor Binghai Yan and Debottam Mandal for the insightful discussions. We thank Professor Giovanni Vignale for the fruitful discussions. We also thank Dr. Atasi Chakraborty and Dr. Subhajit Sinha for providing valuable feedback about the manuscript. K. D. was supported by the Weizmann Institute of Science, Dean of Faculty fellowship, and the Koshland Foundation. K. G. thanks the MHRD, India for funding through the Prime Minister's Research Fellowship. A. A. acknowledges the Department of Science and Technology of the Government of India for financial support via Project No. DST/NM/TUE/QM-6/ 2019(G)-IIT Kanpur.

*daskamal457@gmail.com

†amitag@iitk.ac.in

- [1] I. Žutić, J. Fabian, and S. Das Sarma, Spintronics: Fundamentals and applications, *Rev. Mod. Phys.* **76**, 323 (2004).
- [2] A. Hirohata, K. Yamada, Y. Nakatani, I.-L. Prejbeanu, B. Diény, P. Pirro, and B. Hillebrands, Review on spintronics: Principles and device applications, *J. Magn. Magn. Mater.* **509**, 166711 (2020).
- [3] M. Yamamoto, Y. Shimazaki, I. V. Borzenets, and S. Tarucha, Valley Hall effect in two-dimensional hexagonal lattices, *J. Phys. Soc. Jpn.* **84**, 121006 (2015).
- [4] J. R. Schaibley, H. Yu, G. Clark, P. Rivera, J. S. Ross, K. L. Seyler, W. Yao, and X. Xu, Valleytronics in 2d materials, *Nat. Rev. Mater.* **1**, 16055 (2016).
- [5] S. A. Vitale, D. Nezich, J. O. Varghese, P. Kim, N. Gedik, P. Jarillo-Herrero, D. Xiao, and M. Rothschild, Valleytronics: Opportunities, challenges, and paths forward, *Small* **14**, 1801483 (2018).
- [6] D. Xiao, W. Yao, and Q. Niu, Valley-contrasting physics in graphene: Magnetic moment and topological transport, *Phys. Rev. Lett.* **99**, 236809 (2007).
- [7] R. V. Gorbachev, J. C. W. Song, G. L. Yu, A. V. Kretinin, F. Withers, Y. Cao, A. Mishchenko, I. V. Grigorieva, K. S. Novoselov, L. S. Levitov, and A. K. Geim, Detecting topological currents in graphene superlattices, *Science* **346**, 448 (2014).
- [8] M. Sui, G. Chen, L. Ma, W.-Y. Shan, D. Tian, K. Watanabe, T. Taniguchi, X. Jin, W. Yao, D. Xiao, and Y. Zhang, Gate-tunable topological valley transport in bilayer graphene, *Nat. Phys.* **11**, 1027 (2015).
- [9] Y. Shimazaki, M. Yamamoto, I. V. Borzenets, K. Watanabe, T. Taniguchi, and S. Tarucha, Generation and detection of pure valley current by electrically induced Berry curvature in bilayer graphene, *Nat. Phys.* **11**, 1032 (2015).
- [10] W. Yao, D. Xiao, and Q. Niu, Valley-dependent optoelectronics from inversion symmetry breaking, *Phys. Rev. B* **77**, 235406 (2008).
- [11] T. Cao, G. Wang, W. Han, H. Ye, C. Zhu, J. Shi, Q. Niu, P. Tan, E. Wang, B. Liu, and J. Feng, Valley-selective

- circular dichroism of monolayer molybdenum disulphide, *Nat. Commun.* **3**, 887 (2012).
- [12] K. F. Mak, K. He, J. Shan, and T. F. Heinz, Control of valley polarization in monolayer MoS₂ by optical helicity, *Nat. Nanotechnol.* **7**, 494 (2012).
- [13] H. Zeng, J. Dai, W. Yao, D. Xiao, and X. Cui, Valley polarization in MoS₂ monolayers by optical pumping, *Nat. Nanotechnol.* **7**, 490 (2012).
- [14] Y. Li, J. Ludwig, T. Low, A. Chernikov, X. Cui, G. Arefe, Y. D. Kim, A. M. van der Zande, A. Rigosi, H. M. Hill, S. H. Kim, J. Hone, Z. Li, D. Smirnov, and T. F. Heinz, Valley splitting and polarization by the Zeeman effect in monolayer MoSe₂, *Phys. Rev. Lett.* **113**, 266804 (2014).
- [15] D. MacNeill, C. Heikes, K. F. Mak, Z. Anderson, A. Kormányos, V. Zólyomi, J. Park, and D. C. Ralph, Breaking of valley degeneracy by magnetic field in monolayer MoSe₂, *Phys. Rev. Lett.* **114**, 037401 (2015).
- [16] A. Srivastava, M. Sidler, A. V. Allain, D. S. Lembke, A. Kis, and A. Imamoglu, Valley Zeeman effect in elementary optical excitations of monolayer WSe₂, *Nat. Phys.* **11**, 141 (2015).
- [17] K. F. Mak, K. L. McGill, J. Park, and P. L. McEuen, The valley Hall effect in MoS₂ transistors, *Science* **344**, 1489 (2014).
- [18] C. Li, M. W.-Y. Tu, and W. Yao, Revealing the non-adiabatic and non-Abelian multiple-band effects via anisotropic valley Hall conduction in bilayer graphene, *2D Mater.* **8**, 045012 (2021).
- [19] A. Wild, E. Mariani, and M. E. Portnoi, Optical valley separation in two-dimensional semimetals with tilted Dirac cones, *Sci. Rep.* **13**, 19211 (2023).
- [20] S.-H. Zhang, D.-F. Shao, Z.-A. Wang, J. Yang, W. Yang, and E. Y. Tsymbal, Tunneling valley Hall effect driven by tilted Dirac fermions, *Phys. Rev. Lett.* **131**, 246301 (2023).
- [21] Y. Gao, S. A. Yang, and Q. Niu, Field induced positional shift of Bloch electrons and its dynamical implications, *Phys. Rev. Lett.* **112**, 166601 (2014).
- [22] Y. Gao, Semiclassical dynamics and nonlinear charge current, *Front. Phys.* **14**, 33404 (2019).
- [23] This is reminiscent of the linear valley Hall current in time-reversal symmetric systems, where the anomalous charge Hall response vanishes.
- [24] G. Sundaram and Q. Niu, Wave-packet dynamics in slowly perturbed crystals: Gradient corrections and Berry-phase effects, *Phys. Rev. B* **59**, 14915 (1999).
- [25] S. Lai, H. Liu, Z. Zhang, J. Zhao, X. Feng, N. Wang, C. Tang, Y. Liu, K. S. Novoselov, S. A. Yang, and W.-b. Gao, Third-order nonlinear Hall effect induced by the Berry-connection polarizability tensor, *Nat. Nanotechnol.* **16**, 869 (2021).
- [26] Y. Gao, Y. Zhang, and D. Xiao, Tunable layer circular photogalvanic effect in twisted bilayers, *Phys. Rev. Lett.* **124**, 077401 (2020).
- [27] P. Bhalla, K. Das, D. Culcer, and A. Agarwal, Resonant second-harmonic generation as a probe of quantum geometry, *Phys. Rev. Lett.* **129**, 227401 (2022).
- [28] I. Sodemann and L. Fu, Quantum nonlinear Hall effect induced by Berry curvature dipole in time-reversal invariant materials, *Phys. Rev. Lett.* **115**, 216806 (2015).
- [29] S. Sinha, P. C. Adak, A. Chakraborty, K. Das, K. Debnath, L. D. V. Sangani, K. Watanabe, T. Taniguchi, U. V. Waghmare, A. Agarwal, and M. M. Deshmukh, Berry curvature dipole senses topological transition in a moiré superlattice, *Nat. Phys.* **18**, 765 (2022).
- [30] See Supplemental Material at <http://link.aps.org/supplemental/10.1103/PhysRevLett.132.096302> for (i) theory of second-order nonlinear conductivity, (ii) theory of electric-field-induced orbital magnetic moment, (iii) difference between linear and nonlinear valley Hall effect, (iv) calculation for massive tilted Dirac system, (v) NVHE without tilt, (vi) extrinsic contributions to the valley Hall effect, (vii) experimental probe of nonlinear valley Hall effect, (viii) tight-binding model calculations for strained graphene and organic conductor, and (ix) symmetries and materials for NVHE, which includes Refs. [31–35].
- [31] S. Bhowal and G. Vignale, Orbital Hall effect as an alternative to valley Hall effect in gapped graphene, *Phys. Rev. B* **103**, 195309 (2021).
- [32] I. A. Ado, I. A. Dmitriev, P. M. Ostrovsky, and M. Titov, Anomalous Hall effect with massive Dirac fermions, *Europhys. Lett.* **111**, 37004 (2015).
- [33] Z. Z. Du, C. M. Wang, S. Li, H.-Z. Lu, and X. C. Xie, Disorder-induced nonlinear Hall effect with time-reversal symmetry, *Nat. Commun.* **10**, 3047 (2019).
- [34] C. Ortix, Nonlinear Hall effect with time-reversal symmetry: Theory and material realizations, *Adv. Quantum Technol.* **4**, 2100056 (2021).
- [35] M. Beconcini, F. Taddei, and M. Polini, Nonlocal topological valley transport at large valley Hall angles, *Phys. Rev. B* **94**, 121408(R) (2016).
- [36] C. Wang, Y. Gao, and D. Xiao, Intrinsic nonlinear Hall effect in antiferromagnetic tetragonal CuMnAs, *Phys. Rev. Lett.* **127**, 277201 (2021).
- [37] H. Liu, J. Zhao, Y.-X. Huang, W. Wu, X.-L. Sheng, C. Xiao, and S. A. Yang, Intrinsic second-order anomalous Hall effect and its application in compensated antiferromagnets, *Phys. Rev. Lett.* **127**, 277202 (2021).
- [38] A. Gao *et al.*, Quantum metric nonlinear Hall effect in a topological antiferromagnetic heterostructure, *Science* **381**, 181 (2023).
- [39] F. Mazzola, B. Ghosh, J. Fujii, G. Acharya, D. Mondal, G. Rossi, A. Bansil, D. Farias, J. Hu, A. Agarwal, A. Politano, and I. Vobornik, Discovery of a magnetic Dirac system with a large intrinsic nonlinear Hall effect, *Nano Lett.* **23**, 902 (2023).
- [40] J. Wang, H. Zeng, W. Duan, and H. Huang, Intrinsic nonlinear Hall detection of the Néel vector for two-dimensional antiferromagnetic spintronics, *Phys. Rev. Lett.* **131**, 056401 (2023).
- [41] K. Das, S. Lahiri, R. B. Atencia, D. Culcer, and A. Agarwal, Intrinsic nonlinear conductivities induced by the quantum metric, *Phys. Rev. B* **108**, L201405 (2023).
- [42] C. Xiao, H. Liu, J. Zhao, S. A. Yang, and Q. Niu, thermoelectric generation of orbital magnetization in metals, *Phys. Rev. B* **103**, 045401 (2021).
- [43] C. Xiao, Y. Ren, and B. Xiong, Adiabatically induced orbital magnetization, *Phys. Rev. B* **103**, 115432 (2021).
- [44] The tilt can arise in graphene with uniaxial strain (see Sec. S8 of the Supplemental Material [30] for details).
- [45] N. A. Sinitsyn, A. H. MacDonald, T. Jungwirth, V. K. Dugaev, and J. Sinova, Anomalous Hall effect in a two-dimensional Dirac band: The link between the Kubo-Streda

- formula and the semiclassical Boltzmann equation approach, *Phys. Rev. B* **75**, 045315 (2007).
- [46] M. M. Glazov and L. E. Golub, Skew scattering and side jump drive exciton valley Hall effect in two-dimensional crystals, *Phys. Rev. Lett.* **125**, 157403 (2020).
- [47] M. M. Glazov and L. E. Golub, Valley Hall effect caused by the phonon and photon drag, *Phys. Rev. B* **102**, 155302 (2020).
- [48] R. B. Atencia, D. Xiao, and D. Culcer, Disorder in the nonlinear anomalous Hall effect of \mathcal{PT} -symmetric Dirac fermions, *Phys. Rev. B* **108**, L201115 (2023).
- [49] N. A. Sinitsyn, Q. Niu, J. Sinova, and K. Nomura, Disorder effects in the anomalous Hall effect induced by Berry curvature, *Phys. Rev. B* **72**, 045346 (2005).
- [50] M. F. Borunda, T. S. Nunner, T. Lück, N. A. Sinitsyn, C. Timm, J. Wunderlich, T. Jungwirth, A. H. MacDonald, and J. Sinova, Absence of skew scattering in two-dimensional systems: Testing the origins of the anomalous Hall effect, *Phys. Rev. Lett.* **99**, 066604 (2007).
- [51] T. Cai, S. A. Yang, X. Li, F. Zhang, J. Shi, W. Yao, and Q. Niu, Magnetic control of the valley degree of freedom of massive Dirac fermions with application to transition metal dichalcogenides, *Phys. Rev. B* **88**, 115140 (2013).
- [52] Y. Wang, W. Wei, F. Li, X. Lv, B. Huang, and Y. Dai, Valley polarization caused by crystalline symmetry breaking, *Mater. Horiz.* **8**, 244 (2021).
- [53] The valley polarization can be induced by illumination with a circularly polarized light [17] by applying a static magnetic field [51] or by breaking crystalline symmetries [52].
- [54] S. Sinha, P. C. Adak, R. S. Surya Kanthi, B. L. Chittari, L. D. V. Sangani, K. Watanabe, T. Taniguchi, J. Jung, and M. M. Deshmukh, Bulk valley transport and Berry curvature spreading at the edge of flat bands, *Nat. Commun.* **11**, 5548 (2020).
- [55] NVHE offers an additional experimental advantage over the linear VHE. The experimental detection of the linear VHE in graphene superlattices has been subject to some controversy. It is not clear whether the valley current is carried by the edge states [56–59] or by the bulk states [7–9,60]. In contrast, the NVHE is free from this ambiguity since the valley current contributions are Fermi surface dependent, implying that they originate from the bulk bands.
- [56] W. Yao, S. A. Yang, and Q. Niu, Edge states in graphene: From gapped flat-band to gapless chiral modes, *Phys. Rev. Lett.* **102**, 096801 (2009).
- [57] M. J. Zhu, A. V. Kretinin, M. D. Thompson, D. A. Bandurin, S. Hu, G. L. Yu, J. Birkbeck, A. Mishchenko, I. J. Vera-Marun, K. Watanabe, T. Taniguchi, M. Polini, J. R. Prance, K. S. Novoselov, A. K. Geim, and M. Ben Shalom, Edge currents shunt the insulating bulk in gapped graphene, *Nat. Commun.* **8**, 14552 (2017).
- [58] J. M. Marmolejo-Tejada, J. H. García, M. D. Petrović, P.-H. Chang, X.-L. Sheng, A. Cresti, P. Plecháč, S. Roche, and B. K. Nikolić, Deciphering the origin of nonlocal resistance in multiterminal graphene on hexagonal-boron-nitride with *ab initio* quantum transport: Fermi surface edge currents rather than Fermi sea topological valley currents, *J. Phys.* **1**, 015006 (2018).
- [59] S. Roche, S. R. Power, B. K. Nikolić, J. H. García, and A.-P. Jauho, Have mysterious topological valley currents been observed in graphene superlattices?, *J. Phys.* **5**, 021001 (2022).
- [60] Y. D. Lensky, J. C. W. Song, P. Samutpraphoot, and L. S. Levitov, Topological valley currents in gapped Dirac materials, *Phys. Rev. Lett.* **114**, 256601 (2015).
- [61] M. Hirata, K. Ishikawa, K. Miyagawa, M. Tamura, C. Berthier, D. Basko, A. Kobayashi, G. Matsuno, and K. Kanoda, Observation of an anisotropic Dirac cone reshaping and ferrimagnetic spin polarization in an organic conductor, *Nat. Commun.* **7**, 12666 (2016).
- [62] A. Kobayashi, S. Katayama, Y. Suzumura, and H. Fukuyama, Massless fermions in organic conductor, *J. Phys. Soc. Jpn.* **76**, 034711 (2007).
- [63] M. O. Goerbig, J.-N. Fuchs, G. Montambaux, and F. Piéchon, Tilted anisotropic Dirac cones in quinoid-type graphene and α -(BEDT-TTF)₂I₃, *Phys. Rev. B* **78**, 045415 (2008).
- [64] S.-M. Choi, S.-H. Jhi, and Y.-W. Son, Effects of strain on electronic properties of graphene, *Phys. Rev. B* **81**, 081407(R) (2010).
- [65] Z.-K. Yang, J.-R. Wang, and G.-Z. Liu, Effects of Dirac cone tilt in a two-dimensional Dirac semimetal, *Phys. Rev. B* **98**, 195123 (2018).
- [66] J. Liu, W. Duan, and L. Fu, Two types of surface states in topological crystalline insulators, *Phys. Rev. B* **88**, 241303(R) (2013).
- [67] Y. Tanaka, Z. Ren, T. Sato, K. Nakayama, S. Souma, T. Takahashi, K. Segawa, and Y. Ando, Experimental realization of a topological crystalline insulator in SnTe, *Nat. Phys.* **8**, 800 (2012).
- [68] M. T. Dau, C. Vergnaud, A. Marty, C. Beigné, S. Gambarelli, V. Maurel, T. Journot, B. Hyot, T. Guillet, B. Grévin, H. Okuno, and M. Jamet, The valley Nernst effect in WSe₂, *Nat. Commun.* **10**, 5796 (2019).
- [69] Q.-H. Chen, F.-J. Huang, and Y.-P. Fu, Magnon valley thermal Hall effect in triangular-lattice antiferromagnets, *Phys. Rev. B* **105**, 224401 (2022).
- [70] D. Xiao, G.-B. Liu, W. Feng, X. Xu, and W. Yao, Coupled spin and valley physics in monolayers of MoS₂ and other group-VI dichalcogenides, *Phys. Rev. Lett.* **108**, 196802 (2012).